ELSEVIER

Catalysis Today 82 (2003) 223–232

CATALYSIS TODAY

www.elsevier.com/locate/cattod

Simulation of membrane microreactor for fuel cell with methane feed

Shigeo Goto [a,*], Tomohiko Tagawa [a], Suttichai Assabumrungrat [b], Piyasan Praserthdam [b]

[a] *Department of Chemical Engineering, Nagoya University, Chikusa, Nagoya 464-8603, Japan*
[b] *Department of Chemical Engineering, Research Center on Catalysis and Catalytic Reaction Engineering, Chulalongkorn University, Bangkok 10330, Thailand*

Abstract

Microreactors are composed of channels with a dimension of 1–1000 μm in width and depth. Three types of membrane microreactors for production of electric power by fuel cells with methane feed, i.e. (1) Pd membrane microreactor (Pd-MMR) followed by polymer electrolyte fuel cell (PEFC), (2) oxide-ion conducting solid oxide fuel cell (SOFC) and (3) proton conducting solid oxide fuel cell (H^+-SOFC) were simulated and compared.

The Pd-MMR followed by PEFC was the most effective system for electric power generation compared with the other two types of SOFC although the system was rather complex. However, the performances were dependent on the permeation properties of membranes (Pd, YSZ, perovskite) as well as kinetics of catalysts.

Keywords: Microreactor; Palladium membrane; Polymer electrolyte fuel cell; Solid oxide fuel cell

1. Introduction

Microreactors are composed of channels with a dimension of 1–1000 μm in width and depth. Microtechnology is expected to have many advantages for productions of valuable chemicals and energy [1,2].

Higher heat and mass transfer rates in microfluidic system allow reactions to be performed under more severe conditions compared with conventional reactors. A portable setup is also possible. One of the most attractive applications is micro-fuel cell. It is important to estimate the efficiencies of micro-fuel cell systems and to select the adequate one among the various fuel cell systems under the given conditions.

In this paper, three types of membrane microreactors for production of electric powers by fuel cells with methane feed, i.e. (1) Pd membrane microreactor (Pd-MMR) followed by polymer electrolyte fuel cell (PEFC), (2) oxide-ion conducting solid oxide fuel cell (SOFC) and (3) proton conducting solid oxide fuel cell (H^+-SOFC) were simulated and compared.

2. Models

2.1. Three types of microreactor systems

2.1.1. PEFC system with Pd membrane reactor

Jensen [2] introduced a fabrication sequence of Pd-MMR with a very thin Pd film (0.2 μm). The thin film was once supported on a flat surface of the

* Corresponding author. Tel./fax: +81-52-789-3261.
E-mail address: goto@nuce.nagoya-u.ac.jp (S. Goto).

0920-5861/$ – see front matter © 2003 Elsevier B.V. All rights reserved.
doi:10.1016/S0920-5861(03)00236-0

Nomenclature

D_{H_2}	permeation coefficient of hydrogen through perovskite solid electrolyte (m^2/s)
$F_{CH_4,0}$	feed molar flow rate of methane (mol/s)
$(-\Delta H)_j$	heat of reaction j (J/mol)
J_i	permeation rate of component i (mol/(m^2 s))
k	rate constant (mol/(s kg Pa^n))
K_i	adsorption constant of component i (Pa^{-1})
K_j	equilibrium constant of reaction j (Pa^n)
L	thickness of membrane (μm)
$P_{AIR,CA}$	pressure of air in the cathode side (Pa)
$P_{H_2,SW}$	pressure of hydrogen in the sweep side (Pa)
P_i	pressure of component i (Pa)
$P_{t,AN}$	total pressure in the anode side (Pa)
$P_{t,RE}$	total pressure in the reaction side (Pa)
Per_{H_2}	permeation coefficient of hydrogen through Pd membrane (mol/($Pa^{0.5}$ m s))
r_j	rate of reaction j (mol/(kg s))
R_g	gas constant (8.314 J/(mol K))
S	surface area of membrane (m^2)
T	reaction temperature (K)
W	mass of catalyst (kg)
Watt	electric power based on the heat of reaction (W)
x	dimensionless axial length divided by the total length of reactor (–)
X_{CH_4}	conversion of methane (–)
z_{pre}	length of pre-reactor (m)
z_t	total length of reactor (m)

Greek letters

α	constant for gas–membrane interface resistance (mol/(m^2 s $Pa^{1/2}$))
β	constant for bulk oxide of YSZ resistance (mol/(m s $Pa^{1/4}$))
$\gamma_{H_2O,0}$	the feed molar flow rate ratio of steam to methane ($=F_{H_2O,0}/F_{CH_4,0}$) (–)
γ_i	molar flow rate ratio ($=F_i/F_{CH_4,0}$) (–)
ζ_{pre}	ratio of the length of pre-reactor to the total length of reactor ($=z_{pre}/z_t$) (–)
η_{FC}	efficiency of fuel cell on the heat of reaction ($\eta_{FC} = 0.6$) (–)
η_{OV}	overall efficiency based on the combustion heat of methane (–)

Subscripts

AIR	air
AN	anode side
CA	cathode side
i	component i
j	reaction j
RE	reaction side
SW	sweep side
0	feed

support and then the support was made porous (see Fig. 3 in [2]).

In this study, Pd-MMR with a dimension of 200 μm in width and depth and 1 m in length was adopted.

Fig. 1 shows the cross-sectional view of Pd-MMR. The upper part is the sweep side where a permeated

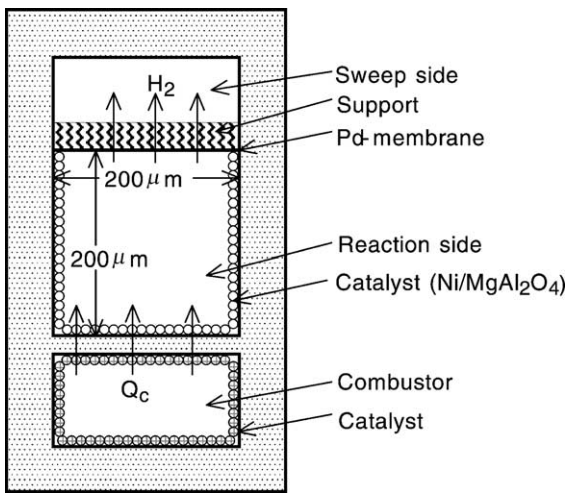

Fig. 1. Cross-sectional view of Pd-membrane microreactor.

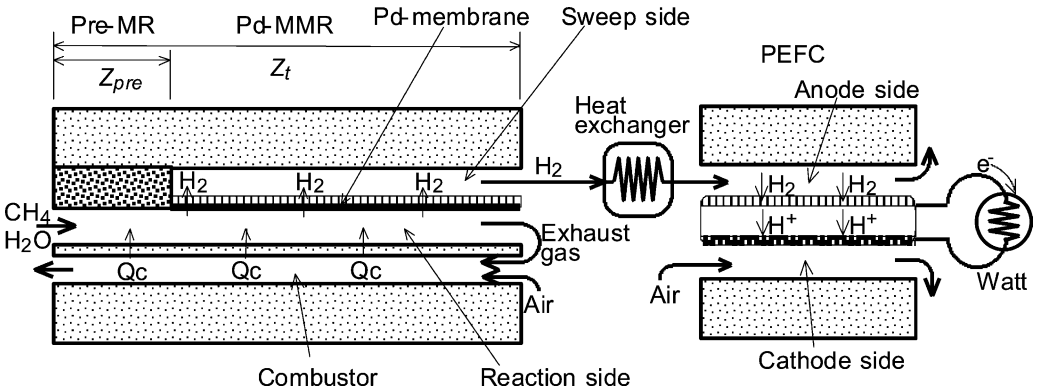

Fig. 2. Concept of Pd-MMR and PEFC.

product H_2 is collected. The middle part is the reaction side where solid catalysts are deposited on both left and right walls and the bottom. The mass of catalyst per surface area is assumed to be 2.85×10^{-3} kg/m^2. Therefore, the total mass of catalyst is $W = 2.85 \times 10^{-3} \times 3 \times 200 \times 10^{-6} = 1.71 \times 10^{-6}$ kg and the surface area of Pd membrane is $S = 200 \times 10^{-6} = 2.0 \times 10^{-4}$ m^2. Then, the ratio S/W becomes 117 m^2/kg. The lower part is the combustor for supplying the heat of combustion (exothermic reactions) to the reaction side (endothermic reactions).

Fig. 2 shows the concept of the total microsystem. Methane and steam are introduced to the reaction side of Pd-MMR. The produced hydrogen is permeated to the sweep side through Pd membrane. The initial part of this microreactor is a conventional microreactor without the membrane (Pre-MR) to avoid back permeation of hydrogen at the front part and to reduce the amount of Pd membrane. The produced hydrogen in the sweep side is cooled down by using a micro-heat exchanger and then introduced to the anode side of PEFC. Air is fed into the cathode side of PEFC. The exhaust gas from the reaction side is burnt with air in the combustor to supply the energy for the strong endothermic steam reforming of methane.

2.1.2. SOFC system

We studied the direct oxidation of dry methane in SOFC [3]. Tompsett et al. [4] described two types of novel applications for micro-SOFCs, namely the combined heat and power system and micro-hybrid vehicles from propane/butane fuels.

Fig. 3 shows the concept of micro-SOFC. The dimensions of micro-SOFC were the same as Pd-MMR. The catalyst, Pt/Al_2O_3 is deposited on the anode side. The mass of catalyst in the anode side is assumed to be the same as Pd membrane reactor.

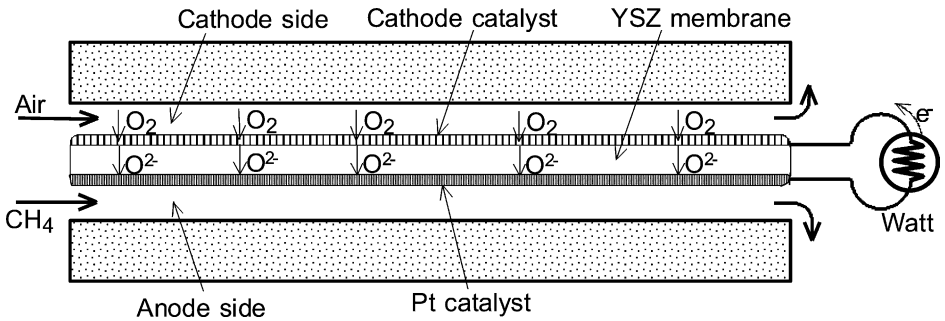

Fig. 3. Concept of micro-SOFC.

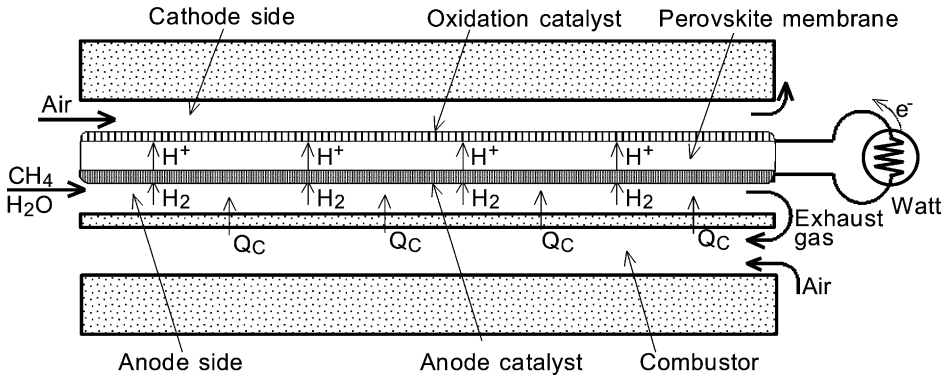

Fig. 4. Concept of micro-H^+-SOFC.

2.1.3. Proton conducting SOFC (H^+-SOFC) system

Although oxide ions are the conducting ions in a conventional SOFC, proton (H^+) is promising for the direct oxidation of produced hydrogen to steam in a microreactor. Bonanos et al. [5] studied the structure and transport properties of perovskite solid electrolytes for fuel cell applications.

Fig. 4 shows the concept of micro-H^+-SOFC. The dimensions of micro-SOFC were the same as Pd-MMR. In the anode (reaction) side, the mass of catalyst, $Ni/MgAl_2O_4$, is assumed to be the same as Pd membrane reactor.

2.2. Kinetics

de Smet et al. [6] studied the partial oxidation of methane to apply production of methanol and hydrogen for fuel cells. Kinetics of combustion of methane, Eq. (1) on Pt/Al_2O_3 were cited from Trimm and Lam [7]

$$CH_4 + 2O_2 \rightarrow CO_2 + 2H_2O$$
$$(-\Delta H)_1 = 837\,\text{kJ/mol} \quad (1)$$
$$r_1 = \frac{k_{1a} P_{CH_4} P_{O_2}}{(1 + K_{CH_4} P_{CH_4} + K_{O_2} P_{O_2})^2} + \frac{k_{1b} P_{CH_4} P_{O_2}^{0.5}}{1 + K_{CH_4} P_{CH_4} + K_{O_2} P_{O_2}},$$
$$k_{1a} = 8.11 \times 10^5 \exp\left(-\frac{86\,000}{R_g T}\right),$$
$$k_{1b} = 6.82 \times 10^5 \exp\left(-\frac{86\,000}{R_g T}\right),$$
$$K_{CH_4} = 0.126 \exp\left(\frac{27\,300}{R_g T}\right),$$
$$K_{O_2} = 7.87 \times 10^{-7} \exp\left(\frac{92\,800}{R_g T}\right)$$

Kinetics of steam reforming of methane, Eqs. (2) and (3) on $Ni/MgAl_2O_4$ were cited from Numaguchi and Kikuchi [8]

$$CH_4 + H_2O \rightarrow CO + 3H_2$$
$$(-\Delta H)_2 = -227\,\text{kJ/mol} \quad (2)$$
$$r_2 = k_2 \frac{P_{CH_4} - P_{CO} P_{H_2}^3 / (K_2 P_{H_2O})}{P_{H_2O}^{0.596}},$$
$$k_2 = 2.62 \times 10^5 \exp\left(-\frac{106\,900}{R_g T}\right)$$

$$CO + H_2O \rightarrow CO_2 + H_2 \quad (-\Delta H)_3 = 33.2\,\text{kJ/mol} \quad (3)$$
$$r_3 = k_3 \left\{ P_{CO} - \frac{P_{CO_2} P_{H_2}}{K_3 P_{H_2O}} \right\},$$
$$k_3 = 2.45 \times 10^2 \exp\left(-\frac{54\,500}{R_g T}\right)$$

The heat of reaction, $(-\Delta H)_j$ ($j = 1, 2, 3$) was determined at 1160 K. The equilibrium constant, K_j ($j = 2, 3$) was estimated from thermodynamic data.

2.3. Permeation rates and mass balances for three types

2.3.1. PEFC system with Pd membrane reactor

The permeation rate of H_2 was estimated by the equation of Hermann et al. [9]

$$J_{H_2} = \left(\frac{\mathrm{Per}_{H_2}}{L}\right)(P_{H_2}^{0.5} - P_{H_2,SW}^{0.5}) \quad (4)$$

$$\mathrm{Per}_{H_2} = 2.19 \times 10^{-4} T^{-1.0358} \exp\left(-\frac{21\,700}{R_g T}\right) \quad (5)$$

By assuming plug flow and isothermal conditions, mass balance equations in the reaction side and the sweep side are given as

$$\frac{d\gamma_i}{dx} = \left\{r_i - \left(\frac{S}{W}\right) J_i\right\}\left(\frac{W}{F_{A,0}}\right) \quad (i = CH_4, H_2O, H_2, CO, CO_2) \quad (6)$$

$$\frac{d\gamma_{H_2,SW}}{dx} = \left(\frac{S}{W}\right) J_{H_2}\left(\frac{W}{F_{A,0}}\right) \quad (7)$$

where the permeation rate of component i except hydrogen is zero ($J_i = 0$) because Pd membrane allows only hydrogen to permeate.

At the entrance ($x = 0$), $\gamma_{CH_4} = 1$, $\gamma_{H_2O} = \gamma_{H_2O,0}$, $\gamma_i = 0$ (products), $\gamma_{H_2,SW} = 0$ (8)

The partial pressures in the reaction side and sweep side can be determined as

$$P_i = \frac{P_{t,RE}\gamma_i}{\sum \gamma_i} \quad (9)$$

$$P_{H_2,SW} = \text{given} \quad (10)$$

The reaction rate of component i can be expressed by stoichiometric relations as follows:

$$r_{CH_4} = -r_2, \quad r_{H_2O} = -r_2 - r_3, \quad r_{H_2} = 3r_2 + r_3, \quad r_{CO} = r_2 - r_3, \quad r_{CO_2} = r_3 \quad (11)$$

2.3.2. SOFC system

The permeation rate of oxygen through yttria stabilized zirconia (YSZ) was estimated by the equations of Han et al. [10].

At gas–membrane interface of cathode side:

$$J_{O_2} = \alpha(P_{O_2,CA}^{1/2} - P_{O_2,a}^{1/2}) \quad (12)$$

In bulk oxide of YSZ:

$$J_{O_2} = \left(\frac{\beta}{L}\right)(P_{O_2,a}^{1/4} - P_{O_2,b}^{1/4}) \quad (13)$$

At membrane–gas interface of anode side:

$$J_{O_2} = \alpha(P_{O_2,b}^{1/2} - P_{O_2}^{1/2}) \quad (14)$$

The constants α and β with wet air in the cathode side were given as follows:

$$\alpha = 4.18 \times 10^{-3} \exp\left(\frac{-53\,000}{R_g T}\right) \quad (15)$$

$$\beta = 5.68 \times 10^{-8} \exp\left(-\frac{72\,000}{R_g T}\right) \quad (16)$$

By assuming plug flow and isothermal, the mass balance equation in the anode side is given as

$$\frac{d\gamma_i}{dx} = \left\{r_i - \left(\frac{S}{W}\right) J_i\right\}\left(\frac{W}{F_{A,0}}\right) \quad (i = O_2, CH_4, H_2O, CO_2) \quad (17)$$

where the permeation rate of component i except for oxygen is zero ($J_i = 0$) because the YSZ membrane allows only oxygen to permeate.

At the entrance ($x = 0$), $\gamma_{CH_4} = 1$, $\gamma_i = 0$ (products) (18)

The partial pressures in the anode side and cathode side can be determined as

$$P_i = \frac{P_{t,AN}\gamma_i}{\sum \gamma_i} \quad (19)$$

$$P_{O_2,CA} = \text{given} \quad (20)$$

Kinetics of Eq. (1) is used for the simulations. For simplicity, the side reactions, Eqs. (2) and (3) are neglected. Therefore, the reaction rate of component i can be expressed by stoichiometric relations as follows:

$$r_{CH_4} = -r_1, \quad r_{O_2} = -2r_1, \quad r_{CO_2} = r_1, \quad r_{H_2O} = 2r_1 \quad (21)$$

Table 1
Standard conditions of micro reactors for three types

System	L (μm)	$F_{CH_4,0}$ (mol/s)	T (K)	Pressure (MPa)	$\gamma_{H_2O,0}$ (–)
Pd-MMR	0.2	2.51×10^{-5}	1160	$P_{t,RE} = 2.55$, $P_{H_2,SW} = 0.1$	1.0
SOFC	0.2	2.12×10^{-7}	1160	$P_{t,AN} = 2.55$, $P_{AIR,CA} = 2.55$	–
H^+-SOFC	0.2	1.95×10^{-5}	1160	$P_{t,AN} = 2.55$, $P_{AIR,CA} = 2.55$	1.0

2.3.3. Proton conducting SOFC (H^+-SOFC) system

The permeation rate of hydrogen through the proton conducting perovskite solid electrolyte was estimated by the equation derived from Kreuer et al. [11]

$$J_{H_2} = \left(\frac{D_{H_2}}{L}\right)\frac{P_{H_2} - P_{H_2,CA}}{R_g T} \quad (22)$$

$$D_{H_2} = 4.42 \times 10^{-7} \exp\left(-\frac{59\,500}{R_g T}\right) \quad (23)$$

The pressure in the cathode (sweep) side, $P_{H_2,CA}$ is assumed to be always zero because the oxidation of hydrogen occurs instantaneously at the cathode surface.

The mass balance equation in the anode side is given as Eq. (6) where the permeation rate of component i except hydrogen is zero ($J_i = 0$) because the perovskite membrane allows only hydrogen to permeate.

$$\text{At the entrance } (x = 0),\ \gamma_{CH_4} = 1,\ \gamma_{H_2O} = \gamma_{H_2O,0},\quad \gamma_i = 0 \text{ (products)} \quad (24)$$

The partial pressures in the anode (reaction) side is given by Eq. (9). Kinetics of Eqs. (2) and (3) are used for the simulations. The stoichiometric relations is the same as Eq. (11).

2.4. Definition of overall efficiency, η_{OV}

The electric power, Watt based on the heat of reaction, Eq. (25) is defined by using the produced hydrogen for the PEFC as Eq. (26)

$$H_2 + \tfrac{1}{2}O_2 \rightarrow H_2O \quad (-\Delta H)_6 = 254.6\,\text{kJ/mol} \quad (25)$$

$$\text{Watt} = \eta_{FC}(-\Delta H)_6 F_{H_2,SW} = \eta_{FC}(-\Delta H)_6 F_{CH_4,0}\gamma_{H_2O,SW} \quad (26)$$

where the efficiency is assumed as $\eta_{FC} = 0.6$.

The overall efficiency based on the combustion heat of methane, Eq. (1), η_{OV} is defined as Eq. (27).

$$\eta_{OV} = \frac{\text{Watt}}{(-\Delta H)_1 F_{CH_4,0}} = \frac{\eta_{FC}(-\Delta H)_6 \gamma_{H_2,SW}}{(-\Delta H)_1} \quad (27)$$

Eqs. (26) and (27) can also be applied to H^+-SOFC system.

In the case of SOFC where the permeated oxygen can be reacted with methane in the anode side, the electric power, Watt and the overall efficiency, η_{OV} are defined as

$$\text{Watt} = \eta_{FC}(-\Delta H)_1 F_{CH_4,0} X_{CH_4} \quad (28)$$

$$\eta_{OV} = \frac{\text{Watt}}{(-\Delta H)_1 F_{CH_4,0}} = \eta_{FC} X_{CH_4} \quad (29)$$

2.5. Standard conditions for simulations

Profiles of molar flow rate ratio γ_i with the dimensionless length x were simulated by using an all-purpose equation solver, EQUATRAN-G (Omega Simulation, Japan).

The standard conditions are listed in Table 1 for three types. The temperature and the pressures of the reaction side were chosen from the upper limits in the kinetic study of Numaguchi and Kikuchi [8].

In the case of SOFC, the pressure of air in the cathode side $P_{AIR,CA}$ is 2.55 MPa. Since the mole fraction of oxygen in the air is 0.21, the pressure of oxygen in the cathode side $P_{O_2,CA} = 2.55 \times 0.21 = 0.536$ MPa. The values of feed molar flow rate of methane, $F_{CH_4,0}$ was selected from the results of optimization in the following sections.

3. Results and discussion

3.1. Effect of pre-microreactor on the profiles in Pd-MMR and PEFC

Fig. 5 shows the simulation results at the standard conditions. Near the entrance, the pressure of hydro-

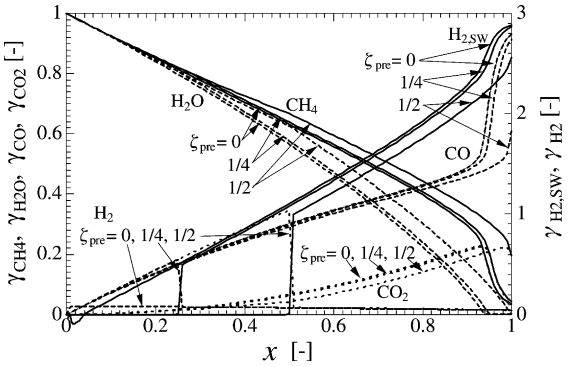

Fig. 5. The effect of pre-microreactor on the profiles at standard condition for PEFC with Pd-MMR.

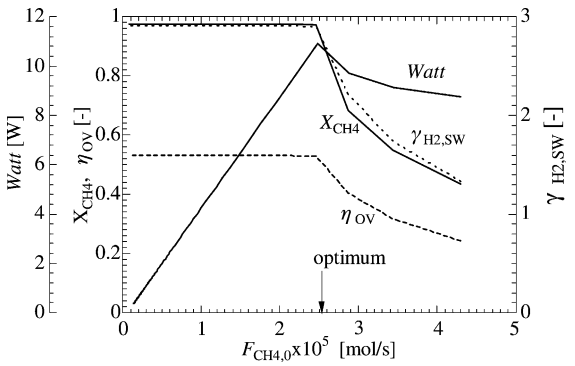

Fig. 6. The effect of $F_{CH_4,0}$ on the values of Watt, η_{OV}, X_{CH_4} and $\gamma_{H_2,SW}$ at the standard condition except for $F_{CH_4,0}$ in PEFC with Pd-MMR.

gen in the reaction side is lower than that in the sweep side and then back permeation occurs. Therefore, a pre-microreactor without Pd membrane may be useful to avoid the back permeation and to reduce the amount of the Pd membrane. The effect of pre-microreactor on the profiles is also shown in Fig. 5 by changing the fraction of pre-microreactor ζ_{pre} ($=z_{pre}/z_t$).

In the case of $\zeta_{pre} = 0$ (without pre-microreactor), $\gamma_{H_2,SW}$ is negative until $x = 0.05$ due to the back permeation. After that, $\gamma_{H_2,SW}$ increases monotonously with the length and rapidly near the exit because the reaction rate of Eq. (2), r_2 is very high due to almost zero partial pressure of steam. The steam consumption is always higher than methane because consecutive reactions, (2) and (3) occur while the reaction (1) does not occur at the standard conditions (no feed of air). Carbon monoxide also increases rapidly near the exit because the reaction (3) does not occur due to the shortage of steam.

In the case of $\zeta_{pre} = 1/4$, there are no significant differences from $\zeta_{pre} = 0$. However, in the case of $\zeta_{pre} = 1/2$, the production of hydrogen in the sweep side, $\gamma_{H_2,SW}$ at the exit decreases. Therefore, we should use the pre-microreactor at 1/4 of the total length.

3.2. Effect of $F_{CH_4,0}$ on the performances

The effects of $F_{CH_4,0}$ on the performances for three types of micro-fuel cell systems, that is, PEFC with Pd-MMR, SOFC and H^+-SOFC are shown in Figs. 6–8, respectively.

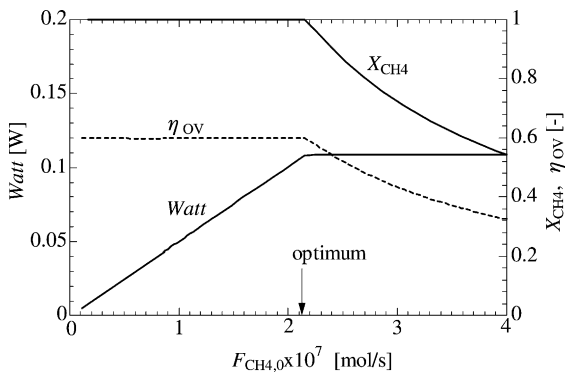

Fig. 7. The effect of $F_{CH_4,0}$ on the values of Watt, η_{OV}, X_{CH_4} and $F_{CH_4,0}$ at the standard conditions except for $F_{CH_4,0}$ in SOFC.

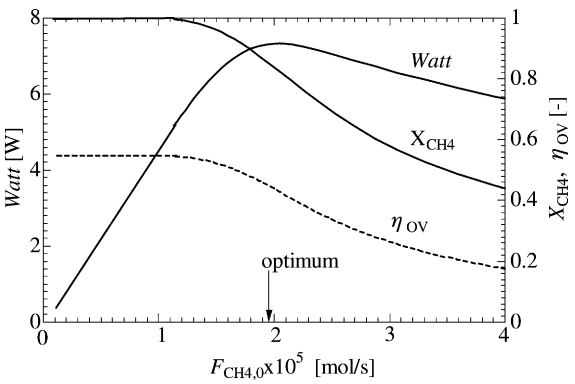

Fig. 8. The effect of $F_{CH_4,0}$ on the values of Watt, η_{OV}, X_{CH_4} and $F_{CH_4,0}$ at the standard conditions except for $F_{CH_4,0}$ in H^+-SOFC.

Fig. 6 shows the effect of $F_{CH_4,0}$ on the values of Watt, η_{OV}, X_{CH_4} and $\gamma_{H_2,SW}$ for PEFC with Pd-MMR system. The simulations were based on the standard condition except that $F_{CH_4,0}$ was varied.

The conversion of methane at the exit of membrane microreactor is given as

$$X_{CH_4} = \frac{F_{CH_4,0} - F_{CH_4}}{F_{CH_4,0}} = 1 - \gamma_{CH_4} \quad (30)$$

The electric power, Watt has a peak at $F_{CH_4,0} = 2.51 \times 10^{-5}$ mol/s which is selected at the standard condition as the optimum. For $F_{CH_4,0} < 2.51 \times 10^{-5}$ mol/s, the values of η_{OV}, X_{CH_4} and $\gamma_{H_2,SW}$ are constant and then Watt is proportional to $F_{CH_4,0}$. For $F_{CH_4,0} > 2.51 \times 10^{-5}$ mol/s, all values decrease.

Fig. 7 shows the effect of $F_{CH_4,0}$ on the values of Watt, η_{OV} and X_{CH_4} for SOFC system. The electric power, Watt and the overall efficiency, η_{OV} are defined as Eqs. (28) and (29). The conversion of methane, X_{CH_4} and the overall efficiency, η_{OV} are 1.00 and 0.60, respectively, until $F_{CH_4,0} = 2.12 \times 10^{-7}$ mol/s and then decrease with the increase in $F_{CH_4,0}$.

The electric power, Watt is proportional to $F_{CH_4,0}$ until $F_{CH_4,0} = 2.12 \times 10^{-7}$ mol/s and then becomes constant. Therefore, the optimum value of $F_{CH_4,0}$ is 2.12×10^{-7} mol/s to avoid methane wastes from the exit.

Fig. 8 shows the effect of $F_{CH_4,0}$ on the values of Watt, η_{OV} and X_{CH_4} for H^+-SOFC system. The electric power, Watt and the overall efficiency, η_{OV} are also defined as Eqs. (26) and (27). The electric power, Watt has a peak at $F_{CH_4,0} = 1.95 \times 10^{-5}$ mol/s although the conversion, X_A is not complete. If the complete conversion is preferable, the feed molar flow rate of methane, $F_{A,0}$ should be reduced to 1.10×10^{-5} mol/s although the electric power, Watt is not at maximum. We select $F_{CH_4,0} = 1.95 \times 10^{-5}$ mol/s as the optimum value where the electric power, Watt has a peak.

3.3. Effect of $\gamma_{H_2O,0}$ on the performances

Fig. 9 shows the effect of $\gamma_{H_2O,0}$ on the values of Watt, η_{OV}, X_{CH_4} and $F_{CH_4,0}$ for PEFC with Pd-MMR system. The feed molar flow rate of methane, $F_{CH_4,0}$ were determined by the same method as Fig. 6 to optimize Watt.

For $\gamma_{H_2O,0} < 1$, the steam is not enough for the complete conversion of methane, X_{CH_4} and then the exhausted gas contains large amounts of methane. However, for $\gamma_{H_2O,0} > 1$, the electric power, Watt decreases with the increase in $\gamma_{H_2O,0}$ because the optimum value of $F_{CH_4,0}$ also decreases. Therefore, $\gamma_{H_2O,0} = 1$ was selected for the standard condition.

3.4. Effect of L on the performances

The effects of L on the performances for PEFC with Pd-MMR, SOFC and H^+-SOFC micro-fuel cell systems are shown in Figs. 10–12, respectively.

For PEFC with Pd-MMR system, Fig. 10 shows the effect of Pd membrane thickness, L on the values of

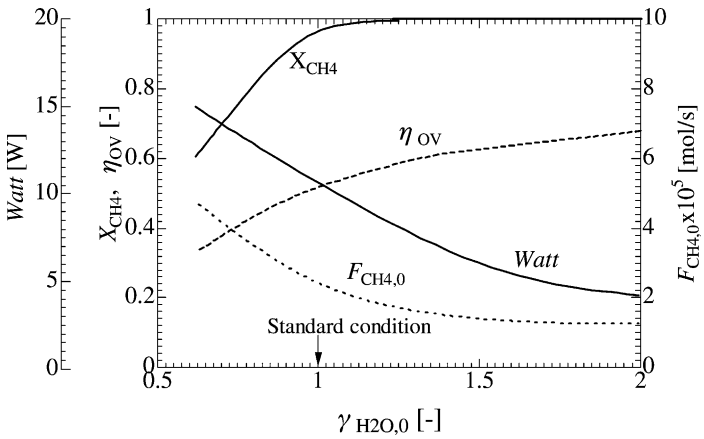

Fig. 9. The effect of $\gamma_{H_2O,0}$ on the values of Watt, η_{OV}, X_{CH_4} and $F_{CH_4,0}$ at the optimized condition for PEFC with Pd-MMR.

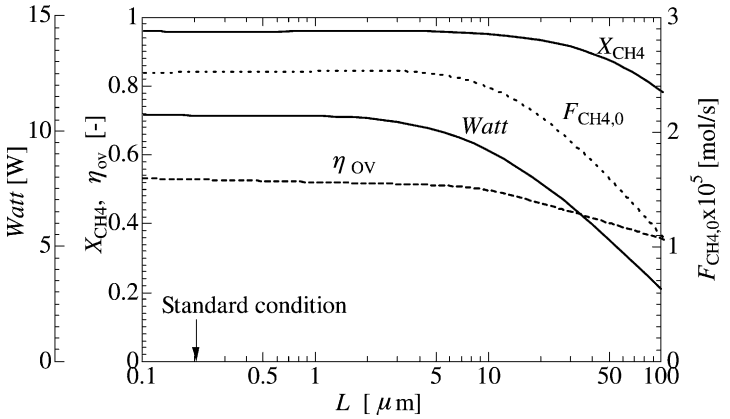

Fig. 10. The effect of L on the values of Watt, η_{OV}, X_{CH_4} and $F_{CH_4,0}$ at the optimized condition for PEFC with Pd-MMR.

Watt, η_{OV}, X_{CH_4} and $F_{CH_4,0}$ at the optimized condition which was determined by the same method as Fig. 6. All values are independent of Pd membrane thickness for $L < 5\,\mu$m while they decrease rapidly for $L > 5\,\mu$m. Therefore, we can use Pd membrane with 5 μm thickness.

The effects of other parameters on the electric power, Watt were also investigated. Higher reaction temperature, higher pressure in the reaction side and lower pressure in the sweep side were always favorable. Total heat balance was considered to recover heat energy by combustion of exhaust gases from Pd-MMR. In any cases, the heat supply was enough.

For SOFC system, Fig. 11 shows the effect of YSZ membrane thickness, L on the values of Watt and $F_{CH_4,0}$ at the optimized condition which was determined by the same method as Fig. 7. The values of X_{CH_4} and η_{OV} are always 1.00 and 0.6 at the optimized conditions, respectively. Two cases of YSZ membrane resistances; namely, three combined resistances of Eqs. (14)–(16) and only one resistance of Eq. (15) were simulated.

For two cases, the electric power, Watt is significantly dependent on the thickness, L which means a high resistance of permeation of oxygen through YSZ and it is much lower than that obtained in the case of Pd-MMR. If the resistances of gas–membrane interfaces, Eqs. (14) and (16) are neglected by using very active catalysts in both sides, the electric power, Watt is improved, especially, for thinner YSZ membranes.

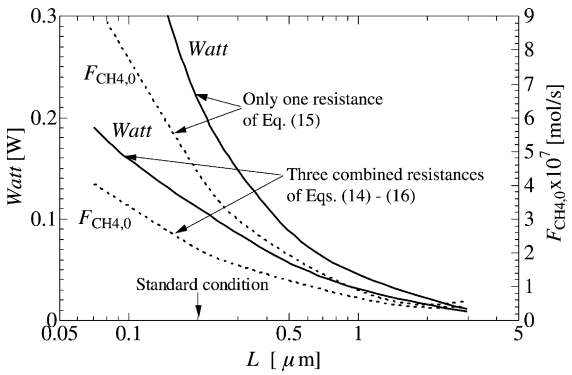

Fig. 11. The effect of L on the values of Watt and $F_{CH_4,0}$ at the optimized condition for SOFC.

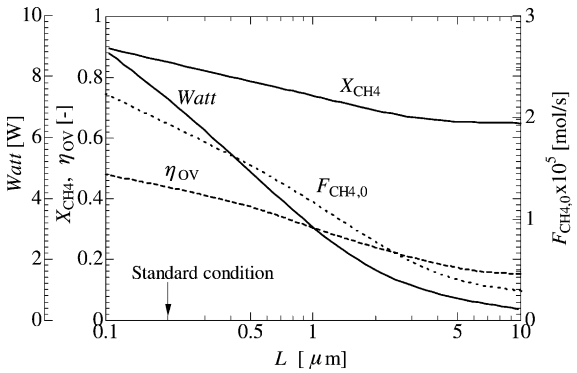

Fig. 12. The effect of L on the values of Watt, η_{OV}, X_{CH_4} and $F_{CH_4,0}$ at the optimized conditions in H^+-SOFC.

This suggests that a micro-SOFC is suitable because a thin YSZ membrane can be used.

For H^+-SOFC system, Fig. 12 shows the effect of perovskite solid electrolyte thickness, L on the values of Watt, η_{OV} and X_{CH_4} and $F_{CH_4,0}$ at the optimized condition which was determined by the same method as Fig. 8.

The electric power, Watt is dependent on the thickness. The thinner membrane is much more effective and then the micro-scale system should be adopted. This proton conducting micro-SOFC was much more effective than the oxide-ion conducting micro-SOFC.

4. Conclusion

Three types of membrane microreactors for production of electric powers by fuel cells with methane feed were simulated and compared.

The Pd-MMR followed by PEFC was the most effective system for electric power generation compared with the other two types of SOFC although the system was rather complex. However, the performances were dependent on the permeation properties of membranes (Pd, YSZ, perovskite) as well as kinetics of catalysts.

Acknowledgements

The supports from TJTTP-JBIC are gratefully acknowledged. The authors also acknowledged Mr. H. Itoh for his technical advice.

References

[1] W. Ehrfeld, V. Hessel, H. Lowe, Microreactors: New Technology for Modern Chemistry, Wiley/VCH, New York, Weinheim, 2000.
[2] K.F. Jensen, Chem. Eng. Sci. 56 (2001) 293.
[3] T. Tagawa, K. Kuroyanagi, S. Goto, S. Assaburumrungrat, P. Prasertham, Chem. Eng. J. 93 (2003) 3.
[4] G.A. Tompsett, C. Finnerty, K. Kendall, T. Alston, N.M. Sammes, J. Power Sour. 86 (2000) 376.
[5] N. Bonanos, K.S. Knight, B. Elli, Solid State Ionics 79 (1995) 161.
[6] C.R.H. de Smet, M.H.J.M. de Croon, R.J. Berger, G.B. Marin, J.C. Schouten, Chem. Eng. Sci. 56 (2001) 4849.
[7] D.L. Trimm, C.W. Lam, Chem. Eng. Sci. 35 (1980) 1405.
[8] T. Numaguchi, K. Kikuchi, Chem. Eng. Sci. 43 (1988) 2295.
[9] C. Hermann, P. Quicker, R. Dittmeyer, J. Membr. Sci. 136 (1997) 161.
[10] J. Han, G. Xomeritakis, Y.S. Lin, Solid State Ionics 93 (1997) 263.
[11] K.D. Kreuer, S. Adams, W. Munch, A. Fuchs, U. Klock, J. Maier, Solid State Ionics 145 (2001) 295.